2021 IEEE 22nd International Workshop on Signal Processing Advances in Wireless Communications (SPAWC) | 978-1-6654-2851-4/21/$31.00 ©2021 IEEE | DOI: 10.1109/SPAWC51858.2021.9593242

Direction Finding with 2D Arrays Using Spatial Sigma-Delta ADCs

Hessam Pirzadeh, Shilpa Rao, and A. Lee Swindlehurst
Center for Pervasive Communications and Computing, University of California Irvine, Irvine, CA 92697, USA.
Email: {hpirzade, shilpar1, swindl

***Abstract*—In many multiple-input multiple-output (MIMO) communication applications, two-dimensional (2D) rectangular arrays are used and the angular field of interest is different in the azimuth and elevation angle domains. In this paper, we show how to exploit scenarios with users confined to narrow elevation angles by means of 2D rectangular arrays with low-resolution spatial $\Sigma\Delta$ sampling in only one (i.e., the vertical) dimension. We analyze the 2D directions-of-arrival (DoA) estimation performance of MUSIC for such arrays, and illustrate the resulting advantage of the $\Sigma\Delta$ approach over standard one-bit receivers.**

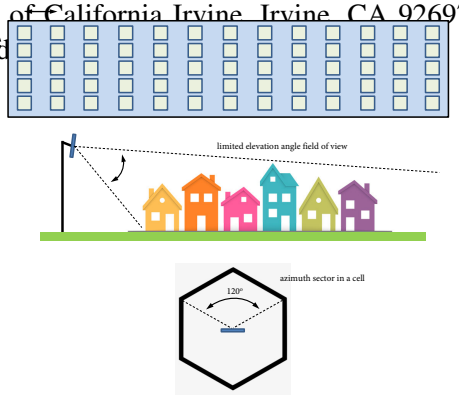

Fig. 1. Angular fields of view in typical wireless cells.

I. Introduction

At millimeter-wave and higher frequencies, wireless channels become highly specular and thus sparse in the angular domain, and channel estimation can be achieved by determining the directions-of-arrival (DoAs) of the users' signals [1]. Most research on DoA estimation has focused on one-dimensional (1D) angle scenarios with linear arrays, but many wireless communication applications employ two-dimensional (2D) arrays where both azimuth and elevation angles are of interest. Although 1D techniques can be easily extended to the generic 2D case, typical 2D scenarios in wireless systems do not have uniform requirements for the angular dimensions. For example, in a classical cellular setup with arrays mounted on a tower or the top of a building, the cell is divided in three azimuthal sectors, and three separate arrays are used to cover each sector. While the desired field of view of each array is relatively wide in azimuth (e.g., 120°), it is relatively narrow in elevation since the most users are on the ground and the strongest gain is needed for distant users at angles near the horizon (see Fig. 1). The same would be true for a 2D array mounted on a wall in a large hall, since most large rooms are much wider/longer than they are tall.

This observation has important consequences in the design of the 2D array, particularly for the case we consider in this paper, where low-resolution spatial Sigma-Delta ($\Sigma\Delta$) analog-to-digital converters (ADCs) are used to quantize the received signals. Low-resolution ADCs have been the subject of considerable work recently for massive MIMO scenarios, with the goal of reducing the cost and complexity of the RF hardware [2]-[6]. Low-resolution spatial $\Sigma\Delta$ sampling provides performance superior to standard quantization in situations where the array is oversampled in space (antennas closer than half-wavelength) or where the DoAs are confined to narrow angular regions, since the quantization noise can be shaped away from the signals of interest [7]-[10].

The case we consider in this paper is the one described above, where the range of elevation angles is limited, but the azimuth angles are not. This suggests a 2D array architecture in which the $\Sigma\Delta$ processing occurs only along the vertical columns of the array, which has an added advantage in that it limits the inherent delay due to daisy-chaining the RF signal between adjacent antennas. Prior work has empirically investigated the 1D DOA estimation performance of a $\Sigma\Delta$-sampled linear array [11], but we derive the analytical 2D DOA performance of this special 2D $\Sigma\Delta$ architecture assuming the DOAs are estimated with the MUSIC [12], [13] algorithm, and we further take into account the effects of mutual coupling.

This work was supported by the National Science Foundation under Grants CCF-1703635 and ECCS-1824565.

II. System Model

A. Channel Model

Consider the uplink of a single-cell multi-user MIMO system where a basestation (BS) equipped with a rectangular array (RA) receives signals from K different directions. Fig. 2 shows the RA oriented to lie in the yz-plane with columns parallel to the z-axis. We assume that the RA has N antennas separated by d_z in each column, and M antennas in each row separated by $d_y = \lambda/2$, where λ is the signal wavelength. We will assume $d_z \leq \lambda/2$ in this work since we will be using $\Sigma\Delta$ sampling along the columns of the array. The origin of the coordinate system coincides with the bottom left antenna of the array. Denote the signal received at the BS by $\boldsymbol{X} \in \mathbb{C}^{N\times M}$ whose mth column is given by

$$\boldsymbol{x}_m = \boldsymbol{G}_m \boldsymbol{s} + \boldsymbol{n}_m, \tag{1}$$

Authorized licensed use limited to: Access paid by The UC Irvine Libraries. Downloaded on August 10,2022 at 15:59:42 UTC from IEEE Xplore. Restrictions apply.

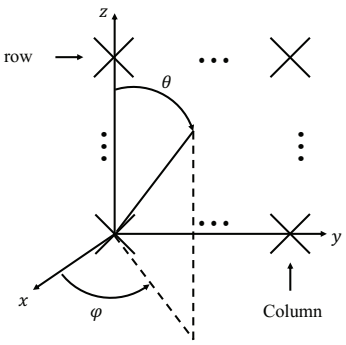

Fig. 2. Rectangular array lying in the yz-plane.

where $\boldsymbol{G}_m = [\boldsymbol{g}_m(\theta_1,\phi_1),\cdots,\boldsymbol{g}_m(\theta_K,\phi_K)] \in \mathbb{C}^{N\times K}$ contains the steering vectors of the K sources for the mth column of the RA. The elements of the $K\times 1$ signal vector $\boldsymbol{s}$ are assumed to be uncorrelated zero-mean Gaussian random variables with diagonal covariance $\mathbb{E}\left\{\boldsymbol{s}\boldsymbol{s}^H\right\} = \mathrm{diag}(p_1,\cdots,p_K)$, and p_k represents the power of the k-th signal arrival. The received noise $\boldsymbol{n}_m$ is also complex zero-mean and Gaussian but with a covariance matrix $\boldsymbol{R}_{\boldsymbol{n}_m}$ that is spatially correlated due to the mutual coupling (MC).

The steering vectors of the array are modeled as

$$\boldsymbol{g}_m(\theta_k,\phi_k) = \boldsymbol{T}\boldsymbol{a}_m(\theta_k,\phi_k)\ ,\ k=1,\cdots,K, \tag{2}$$

where $\boldsymbol{T}$ models the MC and $\boldsymbol{a}_m(\theta_k,\phi_k)$ is the nominal MC-free steering vector assuming an azimuth and elevation DoA of ϕ_k and θ_k, respectively, whose nth element is denoted by

$$[\boldsymbol{a}_m(\theta_k,\phi_k)]_n = e^{-j2\pi\left[(m-1)\frac{d_y}{\lambda}\sin(\phi_k)\sin(\theta_k)+(n-1)\frac{d_z}{\lambda}\cos(\theta_k)\right]},$$

for $m\in\{1,\cdots,M\}$, $n\in\{1,\cdots,N\}$. Since we only consider spatial oversampling along the vertical dimension of the array, we assume that the MC is confined to the antennas in each RA column and not across columns. Our assumed MC model is based on a detailed multiport circuit characterization involving thin dipole antennas [14]. The choice of the circuit parameters that specify $\boldsymbol{T}$ and the noise covariance $\boldsymbol{R}_{\boldsymbol{n}_m}$ can be found in [15], [16], [17].

B. ΣΔ Quantization

In a standard implementation with one-bit quantization, each antenna at the BS is connected to a one-bit ADC. In such systems, the baseband signal at the nm-th antenna becomes

$$y_{nm} = \mathcal{Q}_{nm}(x_{nm})\ , \tag{3}$$

where $\mathcal{Q}_{nm}(.)$ denotes the one-bit quantization operation applied separately to the real and imaginary parts as

$$\mathcal{Q}_{nm}(x_{nm}) = \alpha_{nm}\mathrm{sign}(\mathrm{Re}(x_{nm}))+j\alpha_{nm}\mathrm{sign}(\mathrm{Im}(x_{nm}))\ . \tag{4}$$

The output voltage level of the one-bit quantizers are represented by α_{nm}. While these voltage levels are irrelevant for standard one-bit quantization, in the case of one-bit ΣΔ quantization the selection of appropriate values for α_{nm} is of critical importance, as discussed in [8]. Furthermore, we allow these voltage levels to be a function of the antenna index nm, although once chosen, they remain fixed and independent of the user scenario or channel realization provided that appropriate power control is applied.

As discussed above, in this paper we assume that spatial ΣΔ sampling is only applied in the vertical direction along the index n in each column of the RA. This is because we assume the users are confined to a narrow range of elevation angles (e.g., typically no more than 40° in practice), while the azimuth range is much wider. Thus, we can achieve the benefits of ΣΔ quantization noise shaping without any reduction in antenna spacing in the horizontal dimension, and only a slight reduction in element spacing in the vertical dimension due to the narrow elevation range.

By appropriately designing the output voltages of the ADCs (see [8] for details), the received baseband signal at the BS after column-wise ΣΔ quantization can be represented as

$$\boldsymbol{Y} = \boldsymbol{X} + \boldsymbol{U}^{-1}\boldsymbol{Q}\ , \tag{5}$$

in which

$$\boldsymbol{U} = \begin{bmatrix} 1 & & & \\ e^{-j\psi} & 1 & & \\ \vdots & \ddots & \ddots & \\ e^{-j(M-1)\psi} & \cdots & e^{-j\psi} & 1 \end{bmatrix}, \tag{6}$$

where ψ is used to steer the shaped quantization noise region to the desired DoA, and $\boldsymbol{Q} = [\boldsymbol{q}_1,\cdots,\boldsymbol{q}_M]$ represents the effective quantization noise. Following the same reasoning as in [8], the covariance matrix of each column of quantization noise can be approximated as

$$\boldsymbol{R}_{\boldsymbol{q}_m} \simeq \mathrm{diag}\left(\boldsymbol{p}_{\boldsymbol{q}_m}\right), \tag{7}$$

where

$$\boldsymbol{p}_{\boldsymbol{q}_m} = \left(\frac{\pi}{2}\zeta - 1\right)\boldsymbol{\Pi}\boldsymbol{p}_{\boldsymbol{x}_m} \tag{8}$$

$$\boldsymbol{\Pi} = \begin{bmatrix} 1 & & & & & \boldsymbol{0} \\ \left(\frac{\pi}{2}\zeta-1\right) & 1 & & & & \\ \vdots & \ddots & 1 & & & \\ \left(\frac{\pi}{2}\zeta-1\right)^n & \ddots & \ddots & \ddots & & \\ \vdots & \ddots & \ddots & \ddots & \ddots & \\ \left(\frac{\pi}{2}\zeta-1\right)^{N-1} & \cdots & \left(\frac{\pi}{2}\zeta-1\right)^n & \cdots & \left(\frac{\pi}{2}\zeta-1\right) & 1 \end{bmatrix}$$

$$\boldsymbol{p}_{\boldsymbol{x}_m} = \left[\mathbb{E}\left[|x_{1m}|^2\right],\mathbb{E}\left[|x_{2m}|^2\right],\cdots,\mathbb{E}\left[|x_{Nm}|^2\right]\right]^T\ ,$$

and ζ is a correction factor [17].

Authorized licensed use limited to: Access paid by The UC Irvine Libraries. Downloaded on August 10,2022 at 15:59:42 UTC from IEEE Xplore. Restrictions apply.

III. Quantization Noise Power Density

To evaluate the noise shaping characteristic of the column-wise $\Sigma\Delta$ architecture, we define the quantization noise power density as [8]

$$\rho_q(\theta,\phi) \triangleq \frac{1}{NM}\mathbb{E}\left[\left|\boldsymbol{a}(\theta,\phi)^H \boldsymbol{q}\right|^2\right], \tag{9}$$

where

$$\boldsymbol{a}(\theta,\phi) = \mathrm{vec}\left([\boldsymbol{a}_1,\cdots,\boldsymbol{a}_M]\right) \tag{10}$$

$$\boldsymbol{q} = \mathrm{vec}\left(\boldsymbol{U}^{-1}\boldsymbol{Q}\right). \tag{11}$$

To simplify the calculation of the quantization noise power density, we assume without loss of generality that the $\Sigma\Delta$ array is steered to broadside ($\theta = 90°$). With some algebraic manipulation, $\rho_q(\theta,\phi)$ can be calculated as (12) shown at the top of the next page where $z \triangleq e^{j2\pi\frac{d_z}{\lambda}\cos(\theta)}$. For the sake of analysis, we assume that the elements of the effective quantization noise matrix are uncorrelated. Thus,

$$\rho_q(\theta,\phi) = \frac{1}{NM}\times \sum_{m=1}^{M}\left(4\mathrm{Tr}\left[\boldsymbol{R}_{\boldsymbol{q}_m}\right] - \sigma^2_{q_{Nm}}\right)\sin^2\left(\pi\frac{d_z}{\lambda}\cos(\theta)\right) + \sigma^2_{q_{Nm}}. \tag{13}$$

Eq. (13) demonstrates the noise-shaping capability of column-wise $\Sigma\Delta$ processing on the quantization noise in the elevation angle domain. We can see that for angles near $\theta = 90°$, the first term in (13) is reduced to near zero. In addition, decreasing the antenna spacing d_z/λ also helps to extend the range of θ for which the quantization noise is small. In the following, we study the impact of the quantization noise shaping on DoA estimation performance.

IV. DoA Estimation Performance Analysis

In this section, we investigate the impact of quantization noise on the performance of the MUSIC DoA estimation method. To do so, we re-write the received signal as

$$\boldsymbol{y} = \boldsymbol{G}(\boldsymbol{\theta},\boldsymbol{\phi})\,\boldsymbol{s} + \boldsymbol{n} + \boldsymbol{q}, \tag{14}$$

where $\boldsymbol{\theta} = [\theta_1,\cdots,\theta_K]^T$, $\boldsymbol{\phi} = [\phi_1,\cdots,\phi_K]^T$, the kth column of $\boldsymbol{G}(\boldsymbol{\theta},\boldsymbol{\phi})$ is defined as

$$\boldsymbol{g}_k = \mathrm{vec}\left(\boldsymbol{T}\boldsymbol{a}_1(\theta_k,\phi_k),\cdots,\boldsymbol{T}\boldsymbol{a}_M(\theta_k,\phi_k)\right),$$

$$\boldsymbol{n} = \mathrm{vec}\left(\boldsymbol{n}_1,\cdots,\boldsymbol{n}_M\right),$$

and $\boldsymbol{q}$ is defined in (11). Since the aggregate noise, $\boldsymbol{q}_a = \boldsymbol{n}+\boldsymbol{q}$, is not spatially white, we prewhiten the noise using the matrix $\boldsymbol{W}$ [13]. Hence, the MUSIC cost function becomes

$$f(\theta,\phi) = \mathrm{Tr}\left(\boldsymbol{P}_{\bar{\boldsymbol{g}}}(\theta,\phi)\,\hat{\boldsymbol{E}}_{\boldsymbol{n}}\hat{\boldsymbol{E}}_{\boldsymbol{n}}^H\right), \tag{15}$$

where $\hat{\boldsymbol{E}}_{\boldsymbol{n}}\hat{\boldsymbol{E}}_{\boldsymbol{n}}^H$ represents the estimated noise subspace. In (15), $\boldsymbol{P}_{\bar{\boldsymbol{g}}} = \bar{\boldsymbol{g}}\bar{\boldsymbol{g}}^\dagger$, $\bar{\boldsymbol{g}} = \boldsymbol{W}\boldsymbol{g}$, and $\bar{\boldsymbol{g}}^\dagger = \left(\bar{\boldsymbol{g}}^H\bar{\boldsymbol{g}}\right)^{-1}\bar{\boldsymbol{g}}^H$ is the pseudoinverse of $\bar{\boldsymbol{g}}$. Denote the sample covariance matrix of vectors $\boldsymbol{x}$ and $\boldsymbol{y}$ by

$$\hat{\boldsymbol{R}}_{\boldsymbol{xy}} = \frac{1}{T}\sum_{t=1}^{T}\boldsymbol{x}_t\boldsymbol{y}_t^H, \tag{16}$$

where T denotes the number of snapshots. The matrices $\hat{\boldsymbol{E}}_{\boldsymbol{s}} \in \mathbb{C}^{MN\times K}$ and $\hat{\boldsymbol{E}}_{\boldsymbol{n}} \in \mathbb{C}^{MN\times(MN-K)}$ define the signal and noise subspaces, respectively, and are determined by the eigenvectors of $\boldsymbol{W}\hat{\boldsymbol{R}}_{\boldsymbol{yy}}\boldsymbol{W}^H$. The MUSIC estimate of $(\boldsymbol{\theta},\boldsymbol{\phi})$ is obtained by finding the K local minima of (15). In the next section, we derive an analytical expression for the performance of this estimator for a rectangular array with the column-wise $\Sigma\Delta$ architecture.

A. Estimation Error

To find the covariance matrix of the estimation error, we follow the general approach of [12], [18]. The MUSIC DoA estimate can be obtained by finding the local minima of $f(\theta,\phi)$ in (15) where

$$\nabla f\left(\hat{\theta},\hat{\phi}\right) = \mathbf{0}. \tag{17}$$

Writing the Taylor series expansion of the left-hand side of (17) around the true value (θ,ϕ), we have

$$\nabla f\left(\hat{\theta},\hat{\phi}\right) = \nabla f(\theta,\phi) + \boldsymbol{H}(\theta,\phi)\left(\begin{bmatrix}\hat{\theta}-\theta\\ \hat{\phi}-\phi\end{bmatrix}\right) = \mathbf{0}, \tag{18}$$

where $\boldsymbol{H}(\theta,\phi)$ denotes the Hessian matrix. Hence

$$\begin{bmatrix}\hat{\theta}-\theta\\ \hat{\phi}-\phi\end{bmatrix} = -\boldsymbol{H}^{-1}(\theta,\phi)\,\nabla f(\theta,\phi). \tag{19}$$

Some algebraic manipulation yields the estimation error shown in (20) at the top of the next page, where $f_x \triangleq \partial f/\partial x$, $f_{xx} \triangleq \partial^2 f/\partial x^2$, and $f_{xy} \triangleq \partial^2 f/\partial x\partial y$. Note that replacing θ with ϕ in (20) results in the expression for $\mathbb{E}\left[\left(\hat{\phi}-\phi\right)^2\right]$.

From [20] Eq. (B.3) and (B.5), we have

$$f_\eta = \mathrm{Tr}\left[\frac{\partial \boldsymbol{P}_{\bar{\boldsymbol{g}}}}{\partial\eta}\hat{\boldsymbol{E}}_{\boldsymbol{n}}\hat{\boldsymbol{E}}_{\boldsymbol{n}}^H\right] = 2\mathrm{Re}\left(\mathrm{Tr}\left[\boldsymbol{P}_{\bar{\boldsymbol{g}}}\bar{\boldsymbol{g}}_\eta\bar{\boldsymbol{g}}^\dagger\hat{\boldsymbol{E}}_{\boldsymbol{n}}\hat{\boldsymbol{E}}_{\boldsymbol{n}}^H\right]\right) \tag{21}$$

$$f_{\eta\xi} = \mathrm{Tr}\left[\frac{\partial^2 \boldsymbol{P}_{\bar{\boldsymbol{g}}}}{\partial\eta\partial\xi}\hat{\boldsymbol{E}}_{\boldsymbol{n}}\hat{\boldsymbol{E}}_{\boldsymbol{n}}^H\right] \approx \mathrm{Tr}\left[\frac{\partial^2 \boldsymbol{P}_{\bar{\boldsymbol{g}}}}{\partial\eta\partial\xi}\boldsymbol{E}_{\boldsymbol{n}}\boldsymbol{E}_{\boldsymbol{n}}^H\right] = -2\mathrm{Re}\Bigg(\mathrm{Tr}\Bigg[\Big(\boldsymbol{P}_{\bar{\boldsymbol{g}}}^\perp\bar{\boldsymbol{g}}_\xi\bar{\boldsymbol{g}}^\dagger\bar{\boldsymbol{g}}_\eta\bar{\boldsymbol{g}}^\dagger + \bar{\boldsymbol{g}}^{\dagger^H}\bar{\boldsymbol{g}}_\xi^H\boldsymbol{P}_{\bar{\boldsymbol{g}}}^\perp\bar{\boldsymbol{g}}_\eta\bar{\boldsymbol{g}}^\dagger - \boldsymbol{P}_{\bar{\boldsymbol{g}}}^\perp\bar{\boldsymbol{g}}_{\eta\xi}\bar{\boldsymbol{g}}^\dagger - \boldsymbol{P}_{\bar{\boldsymbol{g}}}^\perp\bar{\boldsymbol{g}}_\eta\left(\bar{\boldsymbol{g}}^H\bar{\boldsymbol{g}}\right)^{-1}\bar{\boldsymbol{g}}_\xi^H\boldsymbol{P}_{\bar{\boldsymbol{g}}}^\perp + \boldsymbol{P}_{\bar{\boldsymbol{g}}}^\perp\bar{\boldsymbol{g}}_\eta\bar{\boldsymbol{g}}^\dagger\bar{\boldsymbol{g}}_\xi\bar{\boldsymbol{g}}^\dagger\Big)\boldsymbol{E}_{\boldsymbol{n}}\boldsymbol{E}_{\boldsymbol{n}}^H\Bigg]\Bigg) \tag{22}$$

where $\eta,\xi \in \{\theta,\phi\}$, $\bar{\boldsymbol{g}}_\eta = \partial\bar{\boldsymbol{g}}/\partial\eta$, $\bar{\boldsymbol{g}}_{\eta\xi} = \partial^2\bar{\boldsymbol{g}}/\partial\eta\partial\xi$, $\boldsymbol{P}_{\bar{\boldsymbol{g}}}^\perp = \boldsymbol{I} - \boldsymbol{P}_{\bar{\boldsymbol{g}}}$, and $\boldsymbol{E}_{\boldsymbol{n}}$ denotes the noise subspace eigenvectors of $\boldsymbol{W}\boldsymbol{R}_{\boldsymbol{yy}}\boldsymbol{W}^H$. To find an expression for the expected values in (20), we can re-write (21) as

$$f_\eta = 2\mathrm{Re}\left(\bar{\boldsymbol{g}}^\dagger\hat{\boldsymbol{E}}_{\boldsymbol{n}}\hat{\boldsymbol{E}}_{\boldsymbol{n}}^H\boldsymbol{P}_{\bar{\boldsymbol{g}}}\bar{\boldsymbol{g}}_\eta\right). \tag{23}$$

Authorized licensed use limited to: Access paid by The UC Irvine Libraries. Downloaded on August 10,2022 at 15:59:42 UTC from IEEE Xplore. Restrictions apply.

$$\rho_q(\theta,\phi) = \frac{1}{NM}\mathbb{E}\left[\left|\sum_{m=1}^{M} e^{-j2\pi(m-1)\frac{d_y}{\lambda}\sin(\phi)\sin(\theta)}\left[\left(1-z^{-1}\right)\sum_{n=1}^{N-1} q_{nm}z^{-(n-1)} + q_{Nm}z^{-(N-1)}\right]\right|^2\right] \tag{12}$$

$$\mathbb{E}\left[\left(\hat{\theta}-\theta\right)^2\right] = \frac{|f_{\phi\phi}|^2\,\mathbb{E}\left[|f_\theta|^2\right] - 2\mathrm{Re}\left(f_{\phi\phi}\mathbb{E}\left[f_\theta f_\phi^*\right] f_{\phi\theta}^*\right) + |f_{\theta\phi}|^2\,\mathbb{E}\left[|f_\phi|^2\right]}{\left|f_{\theta\theta}f_{\phi\phi} - f_{\theta\phi}f_{\phi\theta}\right|^2} \tag{20}$$

In (23), for $T \gg 1$, asymptotic arguments can be used to show that

$$f_\eta = 2\mathrm{Re}\left(\bar{\boldsymbol{g}}^\dagger \hat{\boldsymbol{E}}_{\boldsymbol{n}} \boldsymbol{E}_{\boldsymbol{n}}^H \boldsymbol{P}_{\bar{\boldsymbol{g}}} \bar{\boldsymbol{g}}_\eta\right) \tag{24}$$

$$= 2\mathrm{Re}\left(\sum_{\ell=1}^{MN-K}\left(\bar{\boldsymbol{g}}^\dagger \boldsymbol{E}_{\boldsymbol{s}}\boldsymbol{E}_{\boldsymbol{s}}^H \hat{\boldsymbol{e}}_\ell\right)\left(\boldsymbol{e}_\ell^H \boldsymbol{P}_{\bar{\boldsymbol{g}}}\bar{\boldsymbol{g}}_\eta\right)\right), \tag{25}$$

where $\hat{\boldsymbol{e}}_\ell$ and $\boldsymbol{e}_\ell$ denote the ℓth column of $\hat{\boldsymbol{E}}_{\boldsymbol{n}}$ and $\boldsymbol{E}_{\boldsymbol{n}}$, respectively. Using (24) and the fact that $\mathrm{Re}(u)\,\mathrm{Re}(v) = 1/2\left[\mathrm{Re}(uv) + \mathrm{Re}(uv^*)\right]$ for complex numbers u and v, we arrive at (26) at the top of the next page. Following the same approach as in [12], it can be shown that

$$\bar{\boldsymbol{g}}_k^\dagger \mathbb{E}\left[\boldsymbol{E}_{\boldsymbol{s}}\boldsymbol{E}_{\boldsymbol{s}}^H \hat{\boldsymbol{e}}_\ell \left(\boldsymbol{E}_{\boldsymbol{s}}\boldsymbol{E}_{\boldsymbol{s}}^H \hat{\boldsymbol{e}}_r\right)^T\right] \bar{\boldsymbol{g}}_k^{\dagger T} = 0 \quad \forall \ell, r, \tag{27}$$

$$\bar{\boldsymbol{g}}_k^\dagger \mathbb{E}\left[\boldsymbol{E}_{\boldsymbol{s}}\boldsymbol{E}_{\boldsymbol{s}}^H \hat{\boldsymbol{e}}_\ell \left(\boldsymbol{E}_{\boldsymbol{s}}\boldsymbol{E}_{\boldsymbol{s}}^H \hat{\boldsymbol{e}}_r\right)^H\right] \bar{\boldsymbol{g}}_k^{\dagger H} = \frac{\left(\bar{\boldsymbol{g}}^H\bar{\boldsymbol{g}}\right)^{-2}}{T}\left(\frac{1}{p_k} + \frac{1}{p_k^2}\left[\left(\bar{\boldsymbol{G}}^H\bar{\boldsymbol{G}}\right)^{-1}\right]_{kk}\right)\delta_{\ell r}, \tag{28}$$

$$\bar{\boldsymbol{g}}_\xi^H \boldsymbol{P}_{\bar{\boldsymbol{g}}} \boldsymbol{E}_{\boldsymbol{n}}\boldsymbol{E}_{\boldsymbol{n}}^H \boldsymbol{P}_{\bar{\boldsymbol{g}}} \bar{\boldsymbol{g}}_\eta = \bar{\boldsymbol{g}}_\xi^H \boldsymbol{P}_{\bar{\boldsymbol{g}}}\left(\boldsymbol{I} - \bar{\boldsymbol{G}}\left(\bar{\boldsymbol{G}}^H\bar{\boldsymbol{G}}\right)^{-1}\bar{\boldsymbol{G}}^H\right)\boldsymbol{P}_{\bar{\boldsymbol{g}}}\bar{\boldsymbol{g}}_\eta, \tag{29}$$

where $\bar{\boldsymbol{G}} = \boldsymbol{W}\boldsymbol{G}$ and $\delta_{\ell r}$ is the delta function. Plugging (27)-(29) into (26) leads to (30) at the top of the next page. In the next section, we evaluate the accuracy of this expression and compare the performance of the MUSIC algorithm in the column-wise $\Sigma\Delta$ architecture with that of standard one-bit quantization and infinite resolution ADCs.

V. Numerical Results

We assume static power control [19] so that $p_k = p_0\ \forall k$. Thus, the signal-to-noise ratio (SNR) is defined as

$$\mathrm{SNR} = p_0 \frac{\mathrm{Tr}\left[\boldsymbol{G}\boldsymbol{G}^H\right]}{\mathrm{Tr}\left[\boldsymbol{R}_{\boldsymbol{n}}\right]}. \tag{31}$$

The circuit parameters that define the MC were chosen to be the same as in [15], [16]. We first illustrate how the column-wise $\Sigma\Delta$ architecture is beneficial in shaping the quantization noise. For this experiment, we assume a single source with DoA $(\theta,\phi) = (140^\circ, -30^\circ)$. Therefore, the center angle of the $\Sigma\Delta$ array is steered towards $\psi = 2\pi\frac{d_z}{\lambda}\cos(140^\circ)$. We consider a 10×10 RA with $d_z = \lambda/4$, $d_y = \lambda/2$, and $\mathrm{SNR} = 0$ dB. Fig. 3 shows that the column-wise $\Sigma\Delta$ architecture can significantly alleviate the adverse effect of quantization in both the elevation and azimuth directions compared with standard one-bit quantization. This experiment shows that with only 10 antennas in the vertical direction, the $\Sigma\Delta$ architecture is able to provide considerable quantization noise shaping. This is a promising result since it shows that the benefit of the $\Sigma\Delta$ architecture can be achieved without requiring a long end-to-end delay as the RF signal feedback propagates from one antenna to the next. Moreover, it is consistent with practical implementations where more antenna elements are placed in the horizontal direction for increased azimuth angle resolution.

In the second experiment, we investigate to what extent the column-wise $\Sigma\Delta$ architecture can improve the performance of MUSIC DoA estimates. We assume $K = 5$ sources whose elevation DoA is equal to θ_0, and whose azimuth DoAs are set to $[-10^\circ, -30^\circ, -70^\circ, 40^\circ, 10^\circ]$. The center angle of the $\Sigma\Delta$ array is steered towards $\psi = 2\pi\frac{d_z}{\lambda}\cos(\theta_0)$. In the simulations, we set $\theta_0 = 120^\circ$, $d_z = \lambda/4$, $d_y = \lambda/2$, and the correction factor is $\zeta = 1.13$. We further assume $T = 1000$ snapshots, and 10^3 Monte Carlo trials for the simulations. In Fig. 4, the DoA estimation error is compared for cases with high-resolution ADCs (no quantization), standard one-bit quantization, and using column-wise $\Sigma\Delta$ architecture with one-bit ADCs. It can be seen that the $\Sigma\Delta$ architecture outperforms the standard one-bit architecture for both elevation, θ, and azimuth, ϕ, DoA estimation. In addition, the simulation results closely match the theoretical expressions derived in Section IV-A.

VI. Conclusipon

We have studied the benefit of the spatial $\Sigma\Delta$ architecture for DoA estimation with 2D arrays. We showed that by implementing the $\Sigma\Delta$ approach only in the vertical dimension for limited elevation angle ranges, not only we can avoid the inherent delay due to daisy-chaining the RF signal between adjacent antennas, we can also exploit the $\Sigma\Delta$ noise shaping characteristic in both the azimuth and elevation directions. By taking into account the effect of mutual coupling, we showed that with only 10 antennas in the vertical dimension, we can improve the DoA estimation for both elevation and azimuth DoAs. We also quantified the performance of the MUSIC DoA estimator by deriving analytical expressions for the estimation error and verified its accuracy via simulation.

Authorized licensed use limited to: Access paid by The UC Irvine Libraries. Downloaded on August 10,2022 at 15:59:42 UTC from IEEE Xplore. Restrictions apply.

$$\mathbb{E}\left[f_{\eta_k} f_{\xi_k}\right] = 2\mathrm{Re}\left(\sum_{\ell=1}^{MN-K}\sum_{r=1}^{MN-K}\left(\boldsymbol{e}_\ell^H \boldsymbol{P}_{\bar{\boldsymbol{g}}}\bar{\boldsymbol{g}}_\eta\right)\left(\boldsymbol{e}_r^H \boldsymbol{P}_{\bar{\boldsymbol{g}}}\bar{\boldsymbol{g}}_\xi\right)\left(\bar{\boldsymbol{g}}^\dagger \mathbb{E}\left[\boldsymbol{E_s}\boldsymbol{E_s}^H\hat{\boldsymbol{e}}_\ell\left(\boldsymbol{E_s}\boldsymbol{E_s}^H\hat{\boldsymbol{e}}_r\right)^T\right]\bar{\boldsymbol{g}}^{\dagger T}\right)\right) + 2\mathrm{Re}\left(\sum_{\ell=1}^{MN-K}\sum_{r=1}^{MN-K}\left(\boldsymbol{e}_\ell^H \boldsymbol{P}_{\bar{\boldsymbol{g}}}\bar{\boldsymbol{g}}_\eta\right)\left(\bar{\boldsymbol{g}}_\xi^H \boldsymbol{P}_{\bar{\boldsymbol{g}}}\boldsymbol{e}_r\right)\left(\bar{\boldsymbol{g}}^\dagger \mathbb{E}\left[\boldsymbol{E_s}\boldsymbol{E_s}^H\hat{\boldsymbol{e}}_\ell\left(\boldsymbol{E_s}\boldsymbol{E_s}^H\hat{\boldsymbol{e}}_r\right)^H\right]\bar{\boldsymbol{g}}^{\dagger H}\right)\right) \quad (26)$$

$$\mathbb{E}\left[f_{\eta_k} f_{\xi_k}\right] = \frac{2\left(\bar{\boldsymbol{g}}^H\bar{\boldsymbol{g}}\right)^{-2}}{T}\mathrm{Re}\left(\bar{\boldsymbol{g}}_\xi^H \boldsymbol{P}_{\bar{\boldsymbol{g}}}\left(\boldsymbol{I} - \bar{\boldsymbol{G}}\left(\bar{\boldsymbol{G}}^H\bar{\boldsymbol{G}}\right)^{-1}\bar{\boldsymbol{G}}^H\right)\boldsymbol{P}_{\bar{\boldsymbol{g}}}\bar{\boldsymbol{g}}_\eta\left(\frac{1}{p_k} + \frac{1}{p_k^2}\left[\left(\bar{\boldsymbol{G}}^H\bar{\boldsymbol{G}}\right)^{-1}\right]_{kk}\right)\right) \quad (30)$$

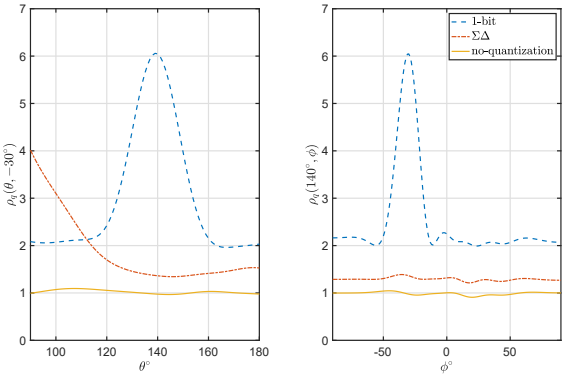

Fig. 3. Aggregate noise power density. $N = 10$, $M = 10$, $d_z = \lambda/4$, SNR $= 0$ dB.

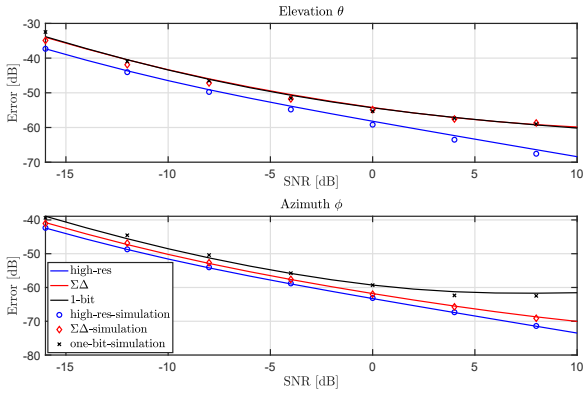

Fig. 4. Estimation error versus SNR. $N = 10$, $M = 10$, $d_z = \lambda/4$, $d_y = \lambda/2$.

REFERENCES

[1] Z. Pi and F. Khan, "An introduction to millimeter-wave mobile broadband systems," *IEEE Commun. Mag.*, vol. 49, no. 6, pp. 101-107, June 2011.

[2] C. Mollén, J. Choi, E. G. Larsson, and R. W. Heath, "Uplink performance of wideband massive MIMO with one-bit ADCs," *IEEE Trans. Wireless Commun.*, vol. 16, no. 1, pp. 87–100, Jan 2017.

[3] J. Zhang, L. Dai, S. Sun, and Z. Wang, "On the spectral efficiency of massive MIMO systems with low-resolution ADCs," *IEEE Commun. Lett.*, vol. 20, no. 5, pp. 842-845, May 2016.

[4] Y. Li, C. Tao, L. Liu, A. Mezghani, G. Seco-Granados, and A. Swindlehurst, "Channel estimation and performance analysis of one-bit massive MIMO systems," *IEEE Trans. Signal Process.*, vol. 65, no. 15, pp. 4075-4089, May 2017.

[5] S. Jacobsson, G. Durisi, M. Coldrey, U. Gustavsson, and C. Studer, "Throughput analysis of massive MIMO uplink with low-resolution ADCs," *IEEE Trans. Wireless Commun.*, vol. 16, no. 6, pp. 4038–4051, June 2017.

[6] Y. Li, C. Tao, A. L. Swindlehurst, A. Mezghani, and L. Liu, "Downlink achievable rate analysis in massive MIMO systems with one-bit DACs," *IEEE Commun. Lett.*, vol. 21, no. 7, pp. 1669–1672, July 2017.

[7] D. Barac and E. Lindqvist, "Spatial sigma-delta modulation in a massive MIMO cellular system," Master's thesis, Department of Computer Science and Engineering, Chalmers University of Technology, 2016.

[8] H. Pirzadeh, G. Seco-Granados, S. Rao, and A. Swindlehurst, "Spectral efficiency of one-bit Sigma-Delta massive MIMO," *IEEE J. Sel. Areas Commun.*, vol. 38, no. 9, pp. 2215–2226, 2020.

[9] M. Shao, W. Ma, Q. Li and A. L. Swindlehurst, "One-Bit Sigma-Delta MIMO Precoding," *IEEE J. Sel. Topics Signal Process.*, vol. 13, no. 5, pp. 1046-1061, Sep. 2019.

[10] S. Rao, H. Pirzadeh and A. Swindlehurst, "Massive MIMO channel estimation with 1-bit spatial Sigma-Delta ADCs," in *Proc. IEEE Int. Conf. Acous., Speech, Signal Process. (ICASSP)*, May 2019, pp. 4484–4488.

[11] R. S. Sankar, and S. Chepuri, "Millimeter wave MIMO channel estimation with 1-bit spatial sigma-delta analog-to-digital converters," in *Proc. IEEE Int. Conf. Acous., Speech, Signal Process. (ICASSP)*, June 2021.

[12] P. Stoica and A. Nehorai, "MUSIC, maximum likelihood, and Cramer-Rao bound," *IEEE Trans. Acoust., Speech, Signal Process.*, vol. 37,no. 5, pp. 720–741, May 1989.

[13] A. L. Swindlehurst and T. Kailath, "A performance analysis of subspacebased methods in the presence of model error—Part I: The MUSIC algorithm," *IEEE Trans. Signal Process.*, vol. 40, pp. 1758–1775, July 1992.

[14] S. A. Schelkunoff, *Antennas: Theory and Practice*. New York: John Wiley and Sons, 1952.

[15] H. Pirzadeh, G. Seco-Granados, A. L. Swindlehurst and J. A. Nossek, "On the Effect of Mutual Coupling in One-Bit Spatial Sigma-Delta Massive MIMO Systems," in *Proc. IEEE 21st International Workshop on Signal Processing Advances in Wireless Communications (SPAWC), Atlanta, GA, USA*, May 2020, pp. 1-5.

[16] H. Pirzadeh, A. L. Swindlehurst and J. A. Nossek, "Space-Constrained Mixed-ADC Massive MIMO," in *Proc. IEEE 20th International Workshop on Signal Processing Advances in Wireless Communications (SPAWC), Cannes, France*, July 2019, pp. 1-5.

[17] S. Rao, G. Seco-Granados, J. A. Nossek, and A. Swindlehurst, "Massive MIMO channel estimation with low-resolution spatial sigma-delta ADCs," arXiv.org Jan. 2021. Available: http://arxiv.org/abs/2005.07752.

[18] P. Stoica, and A. Nehorai, ""Performances study of conditional and unconditional direction of arrival estimation," *IEEE Trans. Acoust., Speech, Signal Process.*, vol. 38, no. 10, pp. 1783-1795, Oct. 1990.

[19] E. Björnson, E. G. Larsson, and M. Debbah, "Massive MIMO for maximal spectral efficiency: How many users and pilots should be allocated?," *IEEE Trans. Wireless Commun.*, vol. 15, no. 2, pp. 1293-1308, Feb. 2016.

[20] M. Viberg, and B. Ottersten, "Sensor array processing based on subspace fitting," *IEEE Trans. Signal Process.*, vol. 39, no. 5, pp. 1110-1121, May 1991.

Authorized licensed use limited to: Access paid by The UC Irvine Libraries. Downloaded on August 10,2022 at 15:59:42 UTC from IEEE Xplore. Restrictions apply.